ADVANCED OPTICAL MATERIALS
www.advopticalmat.de

Strong Coupling in Fully Tunable Microcavities Filled with Biologically Produced Fluorescent Proteins

Christof P. Dietrich, Anja Steude, Marcel Schubert, Jürgen Ohmer, Utz Fischer, Sven Höfling,* and Malte C. Gather**

Strong exciton–photon coupling phenomena and the formation of exciton–polaritons have inspired extensive research over recent years. This has culminated in the discovery of various groundbreaking phenomena in solid-state physics, such as the Bose–Einstein condensation of polaritons,[1,2] Bogoliubov excitations,[3] and integer and half-integer polariton vortices.[4,5] They further hold great potential in mimicking extraordinary physical systems such as integrated circuits[6] or topological insulators.[7] The rich physics is based on the bosonic nature of exciton–polaritons that are able to accumulate in their ground state where they form a condensate. This enables emission of coherent light without the need for population inversion as required in conventional laser structures. Polariton condensates are particularly attractive from a practical perspective as they offer orders of magnitude smaller condensation thresholds (compared to photon lasing thresholds in the same device). Within a condensate, polaritons also have an intrinsic ability to diffuse and propagate (e.g., away from the region in which they have been generated) and can be readily manipulated by external forces.

Gallium arsenide/aluminium arsenide (GaAs/AlAs) is the most commonly employed material platform for studying strong exciton–photon coupling and mirrors, barriers and wells can all be defined in this material. However, when using the GaAs/AlAs platform, experiments on polariton physics require very low temperatures (few Kelvin range) owing to the small exciton binding energy of only a few meV in these materials. The use of organic emitters as active exciton material by contrast offers formation of stable excitons and polaritons at room temperature and far above. The Frenkel excitons in these materials are tightly localized (to one or a few molecules) and often have exciton binding energies of several hundreds of meV. By placing organic semiconductors as active layers into microcavities, exciton–photon coupling strengths of >500 meV have been achieved, thus taking the exciton–photon system into the ultrastrong coupling regime.[8] Polariton condensation was very recently demonstrated for several structurally very different organic systems, including ladder-type conjugated polymers[9], low-molecular weight fluorenes[10], and biologically produced fluorescent proteins (eGFP[11]). In this context, fluorescent proteins (FPs) retain a special position as they offer superior photonic properties in terms of quantum yield (0.6[12] for eGFP compared to 0.43[13] and 0.25[14] for TDAF and MeLPPP, respectively) and singlet–singlet annihilation (SSA).[11] This effect can be explained by the unique molecular structure of fluorescent proteins, which comprises of a chromophore at the center surrounded by a barrel-like arrangement of β-sheets which effectively protect the chromophore from outside influences and from reactions with ambient species. This outstanding morphology manifests itself in a very good overall photostability at high excitation densities. The green-emitting eGFP was the first organic material for which both a first threshold associated with polariton lasing and a second threshold associated with the onset of photon lasing was observed.[11] This effect is well-known for polariton systems[15] but has previously not been observed in organic materials due to issues with material degradation and possibly excessive exciton–exciton annihilation.[9,10]

Here, we substantiate the versatility of fluorescent proteins for polariton physics and demonstrate a fully tunable laminated polariton cavity filled with the green-emitting protein eGFP and the red-emitting protein tdTomato (molecular structures, **Figure 1**A,B). By slightly tilting one of the cavity mirrors with respect to the other, a cavity thickness gradient is realized allowing spectral tuning of polariton states and simultaneous adjustment of photonic and excitonic fractions of distinct polariton modes. In addition, by introducing a gradient in the mixing ratio of the eGFP-tdTomato-blend, one can change the degree of absorption in different spectral regions in a deterministic manner, which enables an effective way of changing the coupling strength in the system (Figure 1C). The combination of these degrees of freedom yields a strongly coupled cavity-blend system that is fully tunable in terms of its photonic and excitonic properties.

eGFP and tdTomato are particularly interesting for photonic experiments because they are among the FPs with the highest quantum yield and photostability. While eGFP is monomeric, tdTomato forms tandem dimers with a flexible interconnection that, in principle, allows any torsion angle between paired dimers. The absorption and emission spectra of eGFP and tdTomato are given in Figure 1D: the absorption spectrum of eGFP (tdTomato) peaks at 2.540 eV (2.238 eV) whereas the

Dr. C. P. Dietrich, Dr. A. Steude, Dr. M. Schubert, Prof. S. Höfling, Prof. M. C. Gather
SUPA
School of Physics and Astronomy
University of St Andrews
North Haugh, KY16 9SS, St Andrews, UK
E-mail: christof.dietrich@physik.uni-wuerzburg.de; sh222@st-andrews.ac.uk; mcg6@st-andrews.ac.uk
Dr. C. P. Dietrich, Prof. S. Höfling
Technische Physik
Universität Würzburg
Am Hubland, Würzburg 97074, Germany
J. Ohmer, Prof. U. Fischer
Institut für Biochemie
Universität Würzburg
Am Hubland, Würzburg 97074, Germany

DOI: 10.1002/adom.201600659

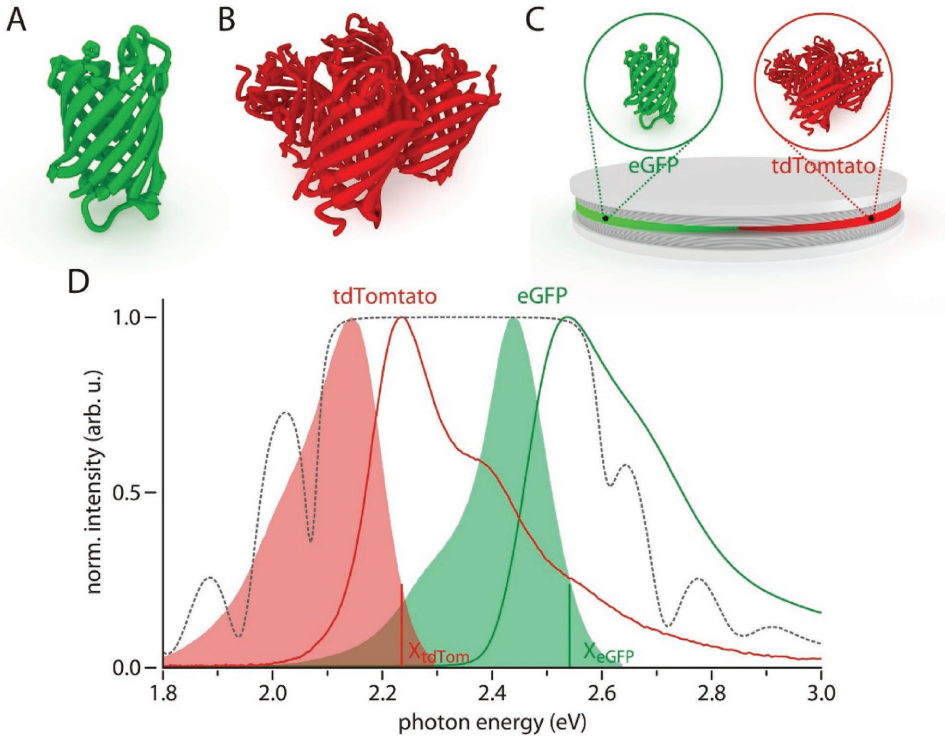

Figure 1. Schematic illustration of the structure of the two biologically produced proteins studied here, A) monomeric eGFP and B) the tandem dimer tdTomato. C) Illustration of the laminated microcavities containing both eGFP and tdTomato. D) Normalized absorption (red and green lines) and emission (red and green areas) spectra of tdTomato (red) and eGFP (green), together with normalized reflectivity spectrum (gray dashed line) of the used dielectric mirrors (center of stop band at 532 nm, corresponding to 2.3 eV). The vertical green and red line highlight the center of the exciton transitions of eGFP and tdTomato, respectively.

emission maximum lies at 2.440 eV (2.144 eV). Spectrally, the absorption of tdTomato overlaps almost perfectly with the emission of eGFP. In solid-state blends of the two FPs, this leads to suppressed emission from eGFP molecules and strong Förster resonant energy transfer (FRET) from eGFP to tdTomato.[16] In general, the efficiency of FRET depends on the intermolecular distance between proteins of different species (R^{-6}-dependence). Typical FRET distances for FP are well below 10 nm.

We first characterized microcavities filled with a film of a homogeneous eGFP-tdTomato-blend (initial concentration is 50 g L^{-1} for eGFP and 5 g L^{-1} for tdTomato in a mixing ratio of 1:1). This was done by measuring the angularly and spectrally resolved white-light reflectivity. Compared to fluorescence measurements, white light reflectance provides a more direct measure of how the absorption bands of the two proteins lead to the hybridization of light and matter state in the structure. In addition, it gives insight into the contribution of all involved modes, that is, both the lower and upper polariton states (the latter are frequently obscured in fluorescence spectra). **Figure 2**A shows the white-light reflectivity spectra for two different cavity thicknesses (1.75 µm, left, and 4.82 µm, right). The measured spectra are TE-polarized and show the spectral region close to the eGFP exciton reservoir. The spectral shift of the modes with angle is extracted from the experimental data and shown in Figure 2B for a magnified section of Figure 2A. None of the involved modes crosses at points along the dispersion curves where the uncoupled modes would be degenerate. This avoided crossing is the key characteristic of the strong coupling regime and is an inherent property of strongly interacting particles. This means that the observed microcavity modes are all of polaritonic nature and can be described as the eigenvalues of a coupled oscillator matrix as previously done in ref. [11] Taking into account the uncoupled excitonic transitions from eGFP and tdTomato (see Figure 1D) and extracting the angular-dependent spectral positions of all observable polariton modes allows deduction of the dispersion of the uncoupled cavity photon modes (shown as dashed gray and black lines in Figure 2B). Not only the regular cavity modes (denoted C*n*) are strongly coupled to the organic excitons but also the first Bragg mode of the dielectric mirrors (denoted B1). We believe this is a consequence of the large quality factor of the cavity which results from the high reflectivity of the mirrors and the good optical homogeneity of the protein blend. From the best fit of a coupled oscillator model to the reflectance spectrum taken at a microcavity thickness of $d = 4.82$ µm, we obtain coupling strengths of $V_1 = 49$ meV to the eGFP excitons and $V_2 = 57$ meV to the tdTomato excitons. The value obtained for eGFP is less than half of what was observed in earlier experiments ($V_1 = 97$ meV[11]). This discrepancy can be explained by the dilution of eGFP with tdTomato and by the different concentrations of the solutions used for the preparation of the protein films (the concentration used here was 50 g L^{-1} whereas 200 g L^{-1} was used in ref. [11]). Generally, the coupling strength scales with the density of molecules in the cavity.[17] Performing

Adv. Optical Mater. **2016**,
DOI: 10.1002/adom.201600659

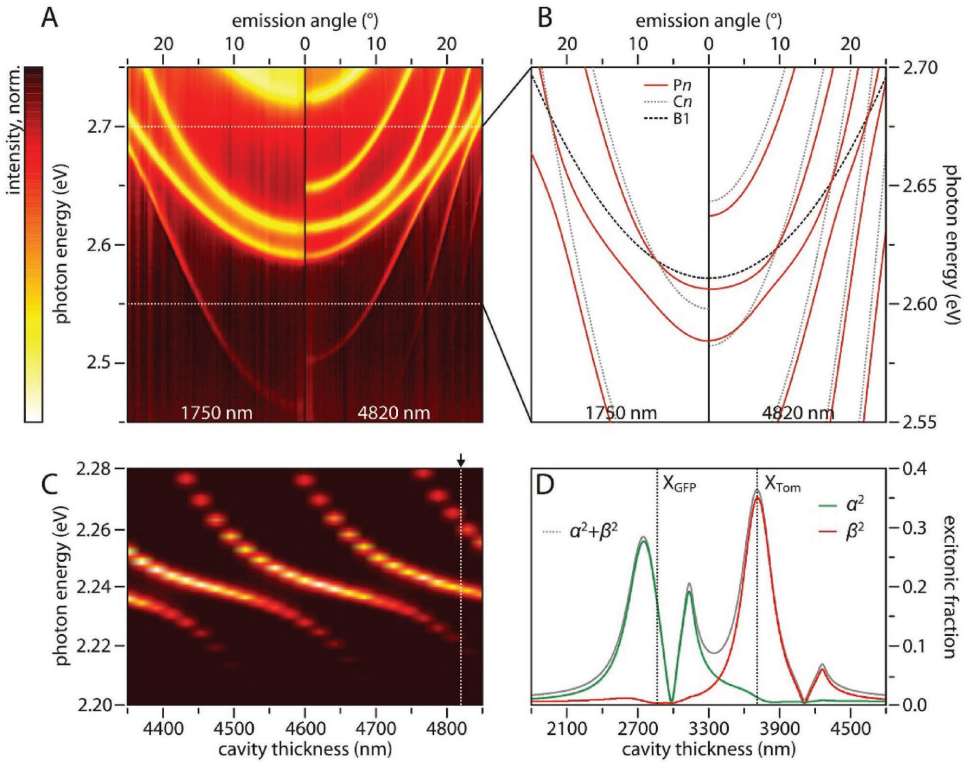

Figure 2. A) Angular-resolved reflectivity spectra of a laminated microcavity filled with a protein blend of eGFP and tdTomato for cavity thicknesses of 1.75 µm (left) and 4.82 µm (right). The spectral range shown coincides with the excitonic range of eGFP. B) Magnified view of (A) showing calculated, uncoupled cavity modes (gray dotted lines) and Bragg modes (black dashed line) as well as coupled polariton modes (red lines). C) Thickness-dependent reflectivity of the laminated microcavity from (A). The black arrow indicates the thickness chosen for the right panel in (A). D) Thickness-dependent excitonic fraction of the main polariton modes of eGFP (α^2) and tdTomato (β^2).

the same fitting routine for a reflectance spectrum taken at a position where the microcavity is much thinner reveals similar values for both coupling strengths, proving that the system remains in the strong coupling regime over the entire lateral extension of the protein microcavity.

Scanning the microcavity along the thickness gradient allows controlled spectral adjustment of the photonic components with respect to the excitonic transitions (so called detuning). Figure 2C shows zero-degree reflectance spectra versus cavity thickness. Changes of detuning dramatically affect the character of each polariton mode, that is, its photonic and excitonic fractions. To visualize this effect in our present configuration, we calculated the excitonic and photonic fractions of a distinct polariton mode starting from the relation $M\,\vec{a} = E^n_{\mathrm{pol}}\,\vec{a}$ with M being the coupled oscillator matrix, $\vec{a} = (\alpha, \beta, \gamma_1, \ldots, \gamma_n)$ being the eigenvectors and En_{pol} being the eigenvalues (polariton mode energies) of the coupled exciton–photon system.[11] The excitonic and photonic fractions of a distinct polariton mode (i.e., an eigenvalue of M) are then given by the squares of the elements of the eigenvectors with $X = \alpha^2 + \beta^2$ being the total excitonic and $C = \gamma_1{}^2 + \cdots + \gamma_n{}^2$ being the total photonic fraction. The thickness dependence of the total excitonic fraction X (as well as the individual excitonic contributions α^2, i.e., associated with eGFP, and β^2, i.e., associated with tdTomato) for a polariton mode crossing both eGFP and tdTomato resonances is shown in Figure 2D. The maximum excitonic fraction observed here is about 0.35, which means that the polariton modes generally are highly photonic. This is a consequence of the large cavity thickness (several times the wavelength of the cavity modes) and the respective collective coupling of several photonic modes to the exciton reservoirs. However, the present tuning mechanism allows creating polariton modes that are either fairly excitonic ($X = 36\%$) or almost fully photonic ($X = 2\%$).

In order to identify the influence of protein intermixing on the coupling mechanism, we pipetted two droplets of pure eGFP and pure tdTomato solution, respectively, to different spots on the bottom mirror, placed several millimeters away from each other. By capping the structure with a top mirror, both droplets intermix substantially but not entirely. Owing to its smaller molecular weight, the monomeric eGFP is considerably more mobile and thus diffuses more quickly than the tandem dimer tdTomato. As a result, we observed that eGFP diffuses into the entire volume of the tdTomato droplet whereas tdTomato only diffuses partially into the eGFP droplet. After drying, the eGFP-tdTomato blend exhibits a protein gradient that ranges from completely unmixed with only monomeric eGFP on one side to partially mixed with eGFP and tdTomato molecules in a (chromophore) mixing ratio of roughly 1:1 on the other side of the sample (see **Figure 3**A). Angular-dependent reflectivity spectra were recorded for different locations across the microcavity along the protein intermixing gradient (Figure 3B–F; the cavity thickness was nearly identical for these spectra). All spectra exhibit avoided crossing between observed modes, indicating strong interaction between protein

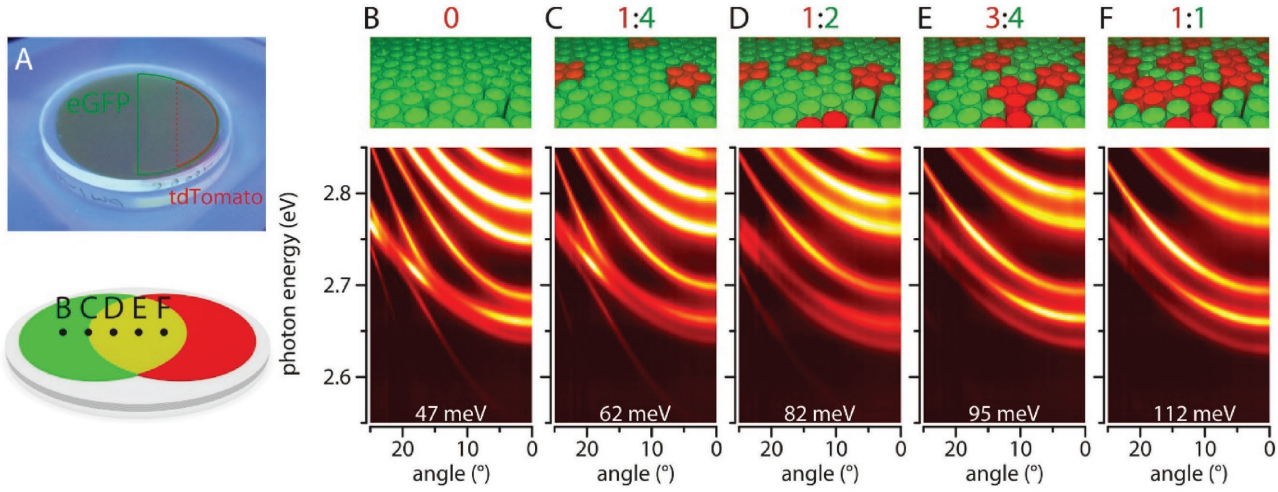

Figure 3. Investigation of a microcavity filled with an eGFP-tdTomato blend of varying mixing ratio. A) (Top) Image of the microcavity under UV illumination. The red and green fluorescence from the two proteins indicates the presence of the gradient in film composition, which ranges from purely eGFP on the left to mixed eGFP-tdTomato on the right hand side. A) (Bottom) Schematic illustration of the microcavity with a gradient in mixing ratio, with indication of where optical measurements were taken. B–F: Angle-resolved TE-polarized reflectivity spectra (at photon energies close to the eGFP exciton energy) for five different blend compositions with nominally B) zero, C) 1:4, D) 1:2, E) 3:4, and F) 1:1 protein mixing ratio (tdTomato:eGFP). Numbers in meV are calculated coupling strengths for each position. Top panels: Schematic of the different mixing ratios of eGFP monomers and tdTomato tandem dimers.

excitons and cavity photons. For the most strongly mixed case (Figure 3G), all observed modes have nearly identical dispersion curvature, indicating an increased coupling strength between excitons and photons. Coupled oscillator fits (similar to those performed for Figure 2D) for all mixing ratios indeed revealed a roughly linear increase in coupling strength with increasing intermixing. The coupling strength V_1 increases from 47 meV in the region containing only eGFP to 112 meV in the region with a fully intermixed eGFP-tdTomato blend (the calculated coupling strengths are given at the bottom of each spectrum in Figure 3). V_2 increases in a similar way from 52 to 120 meV.

This increase in coupling strength can be explained by an increase in oscillator strength, f_{exc} ($V \propto \sqrt{f_{exc}}$ [18]). f_{exc} in turn is a function of the absorption spectrum

$$f_{exc} = \frac{8\pi^2 m\nu}{3e^2 h} D^2 \approx 1.44\times10^{-19} \int \varepsilon_{01}(\nu)\,d\nu \quad (1)$$

with electron mass m, transition dipole moment D, frequency ν, and molar extinction coefficient of the S_0–S_1 transition $\varepsilon_{01}(\nu)$. Since in a blend both eGFP and tdTomato contribute to the photon absorption process, the effective oscillator strength of the blend is enhanced which results in an increased coupling strength.[19,20] For a mixing ratio of 1:1 and taking into account the same chromophore concentration but the different extinction coefficients, quantum yields and absorption spectra (Figure 1D) of both protein species, we estimate a coupling strength of about 102 meV for the fully intermixed blend. This is in good agreement with the experimentally determined value of 112 meV in Figure 3F. Note that this is the result of the increase of the overall molar extinction coefficient, thus enhancing exciton–photon coupling. This means that the coupling strength can be ramped up drastically and in a deterministic manner by mixing tdTomato in defined amounts to the active layer of a strongly coupled microcavity. As pointed out above, the coupling strength can also be tuned by changing the amount of chromophores in the active region. However, changing the number of molecules leads to a change in cavity thickness as the density of molecules in the protein film remains the same. Therefore, changes in coupling strength due to an increased amount of chromophores will always be accompanied by a change in detuning.

Both tuning mechanisms, that is, the thickness and the mixing ratio gradient, can also be combined. **Figure 4** shows a reflectivity scan (normal incidence) over a sample in which the protein and thickness gradients are perpendicular to each other (as illustrated in the top scheme). The scan is performed at a 45° angle with respect to both gradients and shows a

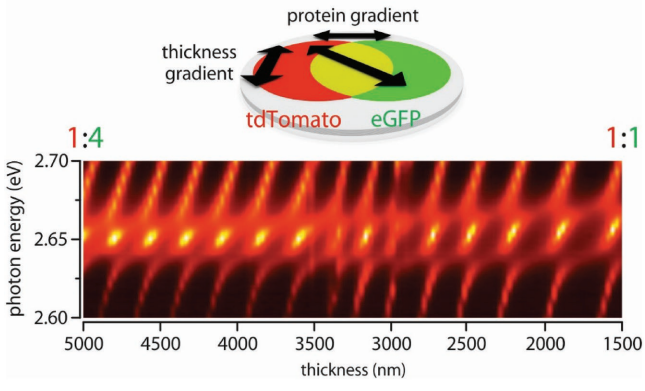

Figure 4. Reflectivity scan (normal incidence) across a microcavity filled with eGFP-tdTomato blend of varying mixing ratio. The scan is performed along both the protein and along the thickness gradient and thus allows simultaneous manipulation of the photonic and excitonic components of polaritons. The estimated mixing ratios at the start and end point of the scan are given by the red and green labels above the plot.

Adv. Optical Mater. **2016**,
DOI: 10.1002/adom.201600659

simultaneous shift of polariton modes across the spectrum as well as an increase in coupling strength (left to right).

In conclusion, we fabricated and investigated laminated microcavities filled with blends of the biologically produced proteins eGFP and tdTomato. The cavities are fully tunable with respect to their photonic and excitonic components. The cavity light field is manipulated by changing the mirror distance along an adjustable gradient in cavity thickness, allowing control of energy separation between cavity and exciton and, thus, determining the character of polaritons from strongly photonic ($C = 98\%$) to fairly excitonic ($X = 36\%$). The addition and intermixing of the red-emitting tdTomato with the green-emitting eGFP enhances protein absorption and increases the exciton–photon coupling. In this way, we were able to demonstrate an enhancement of the coupling strength by about 2.4-fold. This achievement shows the versatility and flexibility of polariton devices. While tuning of photonic state energies can also be achieved in "traditional" photonic components, polariton cavities allow tuning of a mixed light–matter state and also allow adjusting the fraction of the light and the matter component. This offers exciting future possibilities, especially with respect to manipulating the state further by external fields or internal potentials. In this context, our findings represent a major step toward the exploitation and tailoring of polariton condensates in a desired manner inside the very same microcavity.

Experimental Section

The investigated laminated microcavities consist of identical top and bottom dielectric mirrors with ten pairs of SiO_2/Ta_2O_5 layers designed such that the center of the stop band is located at a wavelength of 532 nm and the reflectivity reaches up to 99.97% (the corresponding reflectivity spectrum is shown in Figure 1D). The fluorescent proteins eGFP and tdTomato were expressed in *E. coli* bacteria and purified through column chromatography (details of expression and purification can be found in refs., [11,16] and [21]). The produced protein solutions (2 mL with 4 g L^{-1} protein concentration) are filtered, centrifuged, and desalted in order to reach concentrations of several tens of g L^{-1}. Concentrated solutions of either a single protein and a mixture of both proteins were pipetted onto the bottom mirror and then capped by an identical top mirror. The subsequent drying of the protein leads to the formation of homogeneous solid-state protein films.[11] The mechanical capping allows for the formation of a cavity thickness gradient (changes in cavity thickness typically range from 1 to 5 µm). Reflectivity measurements were performed at room temperature and ambient air conditions. White light is guided to the sample through a microscope objective (40×, NA = 0.55), the reflected light is dispersed in angle by using a Fourier configuration of lenses[22] in the detection path and dispersed in energy using a spectrometer.

Data and materials availability: The research data supporting this publication can be accessed at DOI http://dx.doi.org/10.17630/76b966ca-2378-4626-9d4f-81ba321ec126. Additional data related to this paper may be requested from the authors.

Acknowledgements

The authors thank C. Schneider for fruitful discussions and A. Clemens and K. Ostermann (TU Dresden, Germany) for technical support with protein preparation. The authors acknowledge financial support from the European Research Council (ERC StG ABLASE, 640012), the Scottish Funding Council (via SUPA), the European Union Marie Curie Career Integration Grant (PCIG12-GA-2012-334407), and the EPSRC Hybrid Polaritonics program grant (EP/M025330/1). M.S. acknowledges funding from the German Science Foundation (DFG) through a Research Fellowship (SCHU 3003/1-1) and from the European Commission for a Marie Sklodowska-Curie Individual Fellowship (659213). S.H. gratefully acknowledges support by the Royal Society and the Wolfson Foundation.

Received: August 10, 2016
Revised: September 26, 2016
Published online:

[1] J. Kasprzak, M. Richard, S. Kundermann, A. Baas, P. Jeambrun, J. M. J. Keeling, F. M. Marchetti, M. H. Szymanska, R. André, J. L. Staehli, V. Savona, P. B. Littlewood, B. Deveaud, L. S. Dang, *Nature* **2006**, *443*, 409.
[2] R. Balili, V. Hartwell, D. Snoke, L. Pfeiffer, K. West, *Science* **2007**, *316*, 1007.
[3] S. Utsunomiya, L. Tian, G. Roumpos, C. W. Lai, N. Kumada, T. Fujisawa, M. Kuwata-Gonokami, A. Löffler, S. Höfling, A. Forchel, Y. Yamamoto, *Nat. Phys.* **2008**, *4*, 700.
[4] K. G. Lagoudakis, M. Wouters, M. Richard, A. Baas, I. Carusotto, R. André, L. S. Dang, B. Deveaud-Plédran, *Nat. Phys.* **2008**, *4*, 706.
[5] K. G. Lagoudakis, T. Ostatnický, A. V. Kavokin, Y. G. Rubo, R. André, B. Deveaud-Plédran, *Science* **2009**, *326*, 974.
[6] T. C. H. Liew, A. V. Kavokin, I. A. Shelykh, *Phys. Rev. Lett.* **2008**, *101*, 016402.
[7] A. V. Nalitov, D. D. Solnyshkov, G. Malpuech, *Phys. Rev. Lett.* **2015**, *114*, 116401.
[8] S. Gambino, M. Mazzeo, A. Genco, O. Di Stefano, S. Savasta, S. Patane, D. Ballarini, F. Mangione, G. Lerario, D. Sanvitto, G. Gigli, *ACS Photonics* **2014**, *1*, 1042.
[9] J. D. Plumhof, T. Stöferle, L. Mai, U. Scherf, R. F. Mahrt, *Nat. Mater.* **2014**, *13*, 247.
[10] K. S. Daskalakis, S. A. Maier, R. Murray, S. Kéna-Cohen, *Nat. Mater.* **2014**, *13*, 271.
[11] C. P. Dietrich, A. Steude, L. Tropf, M. Schubert, N. M. Kronenberg, K. Ostermann, S. Höfling, M. C. Gather, *Sci. Adv.* **2016**, *2*, e1600666.
[12] G. Patterson, R. N. Day, D. Piston, *J. Cell Sci.* **2001**, *114*, 837.
[13] S. Kéna-Cohen, S. A. Maier, D. D. C. Bradley, *Adv. Opt. Mater.* **2013**, *1*, 827.
[14] J. Stampfl, S. Tasch, G. Leising, U. Scherf, *Synth. Met.* **1995***71*, 2125.
[15] H. Deng, G. Weihs, D. Snoke, J. Bloch, Y. Yamamoto, *Proc. Natl. Acad. Sci. USA* **2003**, *100*, 15318.
[16] M. C. Gather, S. H. Yun, *Nat. Commun.* **2014**, *5*, 5722.
[17] V. M. Agranovich, M. Litinskaia, D. G. Lidzey, *Phys. Rev. B* **2003**, *67*, 085311.
[18] M. S. Skolnick, T. A. Fisher, D. M. Whittaker, *Semicond. Sci. Technol.* **1998**, *13*, 645.
[19] M. Slootsky, X. Liu, V. M. Menon, S. R. Forrest, *Phys. Rev. Lett.* **2014**, *112*, 076401.
[20] D. M. Coles, N. Somaschi, P. Michetti, C. Clark, P. G. Lagoudakis, P. G. Savvidis, D. G. Lidzey, *Nat. Mater.* **2014**, *13*, 712.
[21] C. P. Dietrich, S. Höfling, M. C. Gather, *Appl. Phys. Lett.* **2014**, *105*, 233702.
[22] C. W. Lai, N. Y. Kim, S. Utsunomiya, G. Roumpos, H. Deng, M. D. Fraser, T. Byrnes, P. Recher, N. Kumada, T. Fujisawa, Y. Yamamoto, *Nature* **2007**, *450*, 529.